INTERNATIONAL JOURNAL FOR NUMERICAL METHODS IN FLUIDS, VOL. 11, 1001–1013 (1990)

THE THERMOCONVECTIVE INSTABILITY OF PLANE POISEUILLE FLOW HEATED FROM BELOW: A PROPOSED BENCHMARK SOLUTION FOR OPEN BOUNDARY FLOWS

G. EVANS

Applied Mechanics Department, Sandia National Laboratories, Livermore, CA 94550, U.S.A.

AND

S. PAOLUCCI

Department of Aerospace and Mechanical Engineering, University of Notre Dame, Notre Dame, IN 46556, U.S.A.

SUMMARY

The transient two-dimensional Navier–Stokes and energy equations have been solved numerically for flow in a horizontal channel heated from below in the Boussinesq limit. For the set of dimensionless parameters chosen, the flow consists of periodic transverse travelling waves resulting from a convective instability. The solution is proposed as a benchmark for the application of outflow boundary conditions (OBC) in time-dependent flows with strong buoyancy effects. Richardson extrapolation in both time and space is used in obtaining the solution. Field plots and profiles of velocity, temperature, vorticity and streamfunction at selected axial positions and times are also presented from the finest grid and smallest time step calculation. The calculations have been made on an extended domain so that the effects of OBC used in the present study would be negligible in the test region.

KEY WORDS Outflow boundary conditions Thermal instability Richardson extrapolation

1. INTRODUCTION

Tremendous advances in fluid mechanics in recent years have been made possible by the use of computers and computer modelling. Much of this progress can be attributed to the rapid evolution of computer technology, specifically the electronics and architecture of computers. Because of size limitations of electronic components, it is generally believed that if advances in computational fluid mechanics are to continue at the current rate, at least in the foreseeable future, new numerical algorithms must be found. One area where such algorithms will have great impact is in the proper formulation of boundary conditions necessary for the numerical solution of fluid mechanics problems that are defined on infinite or semi-infinite regions.

Many problems involving fluid flows require solutions of the mass, momentum and energy conservation equations on some infinite (or semi-infinite) region. For computational reasons the infinite (or semi-infinite) domain is replaced by a finite one and a problem arises concerning how to specify boundary conditions at the artificial boundary. To overcome this difficulty and

0271–2091/90/151001–13$06.50

Received 25 May 1990
Revised 22 June 1990

preserve accuracy, it is often necessary to place the artificial boundary far from the region of interest. This results in a significant increase in both computer storage and computer time. The formulation of 'proper' boundary conditions would allow much more efficient use of computational resources. To this end we propose a benchmark solution that will allow testing of proposed boundary conditions for open channel flows.

The problem is easily defined and general enough in that both forced and natural convection are present and the limiting flow is time-dependent. It consists of a two-dimensional laminar flow in a horizontal channel heated from below under conditions which result in a thermoconvective instability. The problem has immediate engineering relevance, arising in the fabrication of microelectronic circuits using the chemical vapour deposition (CVD) process.[1-6]

In related work, Gage and Reid[7] performed a linear stability analysis of unstably startified plane Poiseuille flow of infinite horizontal extent. They showed that, depending on the values of the dimensionless parameters, the form of the instability could vary from travelling transverse waves, with axes perpendicular to the main flow direction, to longitudinal rolls, with axes aligned with the main flow direction. When the ratio of forced to natural convection forces is small, and provided that the flow is unstable, the flow consists of transverse travelling waves. The thermoconvective instability in the form of travelling transverse waves has been investigated by Luijkx *et al.*,[8] Platten and Legros,[9] Ouazzani *et al.*[10] and Evans and Greif.[11] In a recent numerical study,[11] travelling transverse waves were predicted for conditions typical of CVD in horizontal channel flow reactors. Interest in outflow boundary conditions for time-dependent problems that have strong coupling between the momentum and energy equations has provided the motivation for proposing such a solution as a benchmark.

In the following sections we first define the basic problem and describe the numerical procedure. Then we present the benchmark solution and discuss its accuracy. Finally, additional results obtained from the finest spatial grid and smallest time step solution are presented. It is hoped that this benchmark solution will be used as a vehicle for testing and validating computer programmes that simulate fluid flows with open boundaries. It is further hoped that such stimulus will also lead to the development of new, efficient and accurate algorithms to handle open boundary conditions.

2. PROBLEM DEFINITION

Consider a two-dimensional rectangular channel of height H whose top and bottom walls are respectively maintained at temperatures T_t and T_b, where $T_b > T_t$. The fluid in the channel is initially linearly stratified in temperature and is flowing with a parabolic velocity distribution. At times larger than zero the same velocity and temperature distributions are maintained at the left boundary and the top and bottom solid walls are maintained at temperatures T_t and T_b respectively.

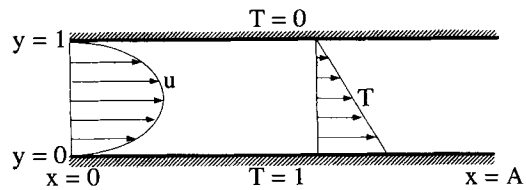

Figure 1. Problem definition

The equations are non-dimensionalized by reference quantities for length, velocity and temperature deviation from T_t by using the channel height H, the average inlet flow speed U_r and the temperature difference $\Delta T = T_b - T_t$ respectively. Time and pressure are then non-dimensionalized by H/U_r and $\rho_b U_r^2$ respectively. The geometry and co-ordinate system are shown in Figure 1.

The problem evolves in time t and is described in two dimensions in terms of the velocity components $v_i=(u, v)$ in the $x_i=(x, y)$ directions, temperature T and pressure P. The non-dimensional Boussinesq equations governing the flow in the channel are given by

$$\frac{\partial v_j}{\partial x_j}=0, \tag{1}$$

$$\frac{\partial v_i}{\partial t}+\frac{\partial}{\partial x_j}(v_j v_i)=-\frac{\partial P}{\partial x_i}-\frac{1}{Fr}Tn_i+\frac{1}{Re}\frac{\partial^2 v_i}{\partial x_j \partial x_j}, \tag{2}$$

$$\frac{\partial T}{\partial t}+\frac{\partial}{\partial x_j}(v_j T)=\frac{1}{Pe}\frac{\partial^2 T}{\partial x_j \partial x_j}, \tag{3}$$

where $n_i=\{0, -1\}$ is the unit vector in the direction of gravity. The initial and boundary conditions, expressed in dimensionless form, are

$$u(x, y, 0)=6y(1-y), \qquad v(x, y, 0)=0, \qquad T(x, y, 0)=1-y, \tag{4}$$

$$\begin{aligned} &u(x, 0, t)=v(x, 0, t)=u(x, 1, t)=v(x, 1, t)=0,\\ &u(0, y, t)=6y(1-y), \qquad v(0, y, t)=0,\\ &T(x, 0, t)=1, \qquad T(x, 1, t)=0, \qquad T(0, y, t)=1-y. \end{aligned} \tag{5}$$

The relevant independent dimensionless parameters appearing in the problem are the Reynolds number, the Froude number and the Peclét number:

$$Re=U_r H/\nu, \qquad Fr=U_r^2/\beta g \Delta T H, \qquad Pe=U_r H/\alpha. \tag{6}$$

In the above definitions ν and α are the kinematic viscosity and thermal diffusivity respectively, β is the coefficient of volume expansion and g is the magnitude of the gravitational field.

The equations actually solved[11] account for variable properties. In those equations the additional temperature overheat parameter $\varepsilon=(T_b-T_t)/T_t$ appears. In the limit $\varepsilon \to 0$ (and with obvious changes in the non-dimensionalization) those equations reduce to (1)–(3), which are the relevant equations in the Boussinesq limit. All reported results have been obtained with $\varepsilon=10^{-4}$ and we have verified that solutions for values of ε as large as 0·0333 differ from the reported solutions by less than 1%. The benchmark solution was obtained for the following values of the parameters: $Re=10$, $Fr=1/150$, and $Pr=Pe/Re=2/3$, where Pr is the Prandtl number.

3. NUMERICAL PROCEDURE

The numerical scheme employed is based on finite differences using a staggered mesh. The finite difference equations are obtained by overlaying a staggered grid network on the region of interest. The differential equations (1)–(3) with initial and boundary conditions (4) and (5) are integrated over local two-dimensional grid control volumes and finite differences are used to discretize the derivatives. All scalar variables are defined at the centre of the volumes, u is defined at the centre of their vertical sides and v is defined at the centre of their horizontal sides. A central difference formulation is used for all spatial derivatives and a backward Euler method is applied to the time derivatives.

The fluid velocity is prescribed on the numerical boundaries of the channel. At those points lying on a boundary we fix the corresponding velocity component to have the desired value, e.g. $v=0$ at $y=0$, 1. The other component of velocity and temperature points do not lie on the boundary. Hence by quadratic interpolation we force two interior points and a fictitious point exterior to the boundary to yield a zero velocity, a constant temperature or a zero flux where appropriate.

Boundary conditions are specified at the channel entry and top and bottom walls. Proper conditions at the outflow end are not known. However, for computational purposes, conditions need to be specified there. We take the computed channel length L to be two times the longest domain proposed for testing OBC and apply the incorrect but usual zero-derivative boundary conditions there. This introduces an additional dimensionless parameter in the problem,

$$A=L/H. \tag{7}$$

We emphasize that this parameter arises only because of our need to solve a finite region on the computer, and the solution within the computed region should not depend on the size of A provided it is large enough to contain several travelling waves (see below).

The solution method is semi-implicit and is based on the TEACH code.[12] The momentum and energy equations are solved implicitly along lines that are normal to the channel surfaces and the equation for pressure is solved implicitly along lines both normal and parallel to the channel surfaces in an alternating fashion. The SIMPLER method described by Patankar[13] is used to determine the pressure field. Underrelaxation factors of 0·9 and 0·8 are used in the solution of the momentum and energy equations respectively. There is no underrelaxation of the pressure equation. At each time step, to obtain an accurate transient solution, the equations are iterated until the following convergence criteria are achieved: at each grid point and for each dependent variable the relative and absolute changes from one iteration to the next must be less than 5×10^{-4} and 1×10^{-4} respectively. The residuals of the equations (absolute values summed over the grid and normalized by the number of control volumes) are also checked and typical values at convergence are between 10^{-4} and 10^{-5}. Global energy and momentum balances are within 1% at each time step. The sufficiency of these criteria has been checked and was reported previously.[11]

In all cases the calculations were continued until the effects of the initial conditions were negligible. This was determined by integrating equations (1)–(3) until the time average of the spatially averaged Nusselt numbers on the bottom (b) and top (t) surfaces of the channel changed by less than 0·1%. The time-averaged Nusselt numbers are defined as

$$\langle \overline{Nu}_{b,t} \rangle \equiv \frac{1}{t_2-t_1}\int_{t_1}^{t_2} \overline{Nu}_{b,t}\,dt, \tag{8}$$

where t_2-t_1 is a time interval that is large compared to the period of the oscillation and

$$\overline{Nu}_{b,t} \equiv \frac{1}{A}\int_0^A Nu_{b,t}\,dx, \tag{9}$$

$$Nu_{b,t} \equiv -\left.\frac{\partial T}{\partial y}\right|_{b,t}. \tag{10}$$

For example, for the finest grid and smallest time step we used $t_2-t_1=6$ and 12, where t_2 is the time at the end of the computation. The variations of the local quantities u_{max} and v_{max}, the maximum values of the horizontal and vertical components of velocity respectively, over these time intervals were also determined to be less than 0·1%.

As noted above, the domain that is being simulated is infinite but for computational economy must be restricted. In the present problem, to adequately simulate the relevant physics consisting of the travelling wave instability, the domain should be large enough to include the initial formation of the instability, several wave cycles and whatever additional length (hopefully short) is necessary to account for effects of the application of the outflow boundary conditions. Since one to two channel heights are necessary for the initial wave development and the wavelength was found to be approximately 1·5, it seems appropriate to restrict the region of interest to $0 \leqslant x \leqslant 10$ for the present problem. Furthermore, because we are applying simple zero-axial-derivative boundary conditions and do not want the effects of these incorrect conditions to affect the region of interest, we have simulated a channel with $A = 20$. To verify that $A = 20$ is sufficient, we made detailed comparisons of the wavelength of the thermal instability, λ, and the maximum of the vertical component of velocity, v_{max}, throughout the channel in two cases, (1) $A = 10$ and (2) $A = 20$, both with $(\Delta x, \Delta y, \Delta t) = (0{\cdot}1,\ 0{\cdot}05,\ 0{\cdot}05\sqrt{Fr})$. Specifically, we found that in the region $2 \leqslant x \leqslant 8$ the values of these quantities agreed to better than 0·3%. Not only was the deviation between the cases within the stated amount but also the variation of the quantities within each case was within this tolerance. For case (2) this level of agreement extended from $2 \leqslant x \leqslant 18$. Owing to differences in the non-dimensionalization discussed in Section 2, we present the time step in a manner that shows the values we actually used.

4. BENCHMARK SOLUTION

Richardson extrapolation in both time and space was used to obtain the benchmark solution. Using the result of computation i for a given dependent variable f_i, the exact value f is assumed obtainable from the formula

$$f = f_i + c_1 \Delta t_i^m + C_1' \Delta x_i^n + C_1'' \Delta y_i^n + \cdots \tag{11}$$

It can be easily shown that for our numerical scheme $m = 1$ and $n = 2$. In other words, the scheme is first-order-accurate in time and second-order-accurate in space. Then we can rewrite

$$f_i = f - (c_1 \Delta t_i + c_2 \Delta t_i^2 + c_3 \Delta t_i^3 + \cdots) - (C_1 \Delta x_i^2 + C_2 \Delta x_i^4 + C_3 \Delta x_i^6 + \cdots), \tag{12}$$

where $C_j = C_j' + C_j'' \gamma^{2j}$ and $\gamma = \Delta y_i / \Delta x_i$. The grid aspect ratio γ is kept constant for all computations with a value of 1/2. Five independent computer runs were made, three that varied the time step by factors of two and three that varied the spatial grid size by factors of $\sqrt{2}$ (one run was common to both of these variations). Using the five independent computations we are able to write five independent equations allowing us to eliminate c_1, c_2, C_1 and C_2 and to obtain the extrapolated value

$$f_e = f - (c_3 \Delta t^3 + \cdots) - (C_3 \Delta x^6 + \cdots). \tag{13}$$

The extrapolated result is third-order-accurate in time and sixth-order-accurate in space. Note that c_j and C_j depend on time and space derivatives respectively evaluated at the same time and spatial location as the function f_i. In order for the extrapolation to be accurate, c_j and C_j should be approximately constant. This is only possible if values of Δt_i and Δx_i are chosen sufficiently small as to give a good representation of the solution.

The results from the individual computations and the extrapolated benchmark solution are presented in Table I, where τ is the temporal period of the oscillation. The quantities shown in Table I were those deemed to be of most interest and/or that best characterize the problem. We point out that the intermediate spatial grid spacing $\Delta x = 0{\cdot}1/\sqrt{2}$ was approximated using 285 x-grid lines and the corresponding $\Delta y = 0{\cdot}05/\sqrt{2}$ was approximated with 30 y-grid lines. As a

Table I. Numerical and extrapolated results

	$[\Delta x, \Delta t]$					
	$[0{\cdot}1, 0{\cdot}2\sqrt{Fr}]$	$[0{\cdot}1, 0{\cdot}1\sqrt{Fr}]$	$[0{\cdot}1, 0{\cdot}05\sqrt{Fr}]$	$[0{\cdot}1/\sqrt{2}, 0{\cdot}05\sqrt{Fr}]$	$[0{\cdot}05, 0{\cdot}05\sqrt{Fr}]$	Extrapolated
τ	1·2544	1·2618	1·2669	1·2901	1·3064	1·3319
λ	1·3526	1·3549	1·3571	1·4006	1·4221	1·4465
$\langle Nu \rangle$	2·549	2·583	2·604	2·568	2·551	2·5583
u_{max}	3·9520	4·0277	4·0583	4·2115	4·2901	4·3958
$y\|_{u_{max}}$	0·8033	0·8056	0·8047	0·8039	0·8047	0·8040
u_{min}	−2·4102	−2·4879	−2·5337	−2·6137	−2·6495	−2·7329
$y\|_{u_{min}}$	0·1353	0·1361	0·1366	0·1378	0·1402	0·1444
v_{max}	4·7501	4·8625	4·9076	4·9507	4·9724	5·0319
$y\|_{v_{max}}$	0·5109	0·5119	0·5124	0·5107	0·5098	0·5094
v_{min}	−4·7670	−4·8611	−4·9192	−4·9511	−4·9709	−5·0587
$y\|_{v_{min}}$	0·4896	0·4881	0·4873	0·4892	0·4903	0·4907

result there are small deviations in the x- and y-grid positioning of 0·05% and 1·0% respectively from the desired values for the application of Richardson extrapolation to three independent spatial solutions applied to the same location. On the basis of the maximum variation of the dependent variables, we estimate that these deviations result in a maximum uncertainty of 1% in the values reported in Table I.

The results of the extrapolation shown in Table I are approximately within 1%–2% of the finest grid and smallest time step solution for all values. We believe that this variation represents an upper bound on the error of the extrapolated results.

We note that because the time step size has been treated as an independent parameter from the spatial step size in the extrapolation procedure, it is not possible to show simply the rate of convergence or the error of the solution by plotting these quantities as a function of grid spacing in the usual manner.[14,15] From Table I it can be seen that moving from left to right along any row, the variable changes as either the time step or the spatial grid is refined. The changes are monotonic with refinement of either the time step or the spatial step, but not necessarily monotonic when both are refined.

One interesting physical observation is that the thermal wave speed $\lambda/\tau = 1{\cdot}09$ is greater than unity, indicating that the rolls move faster than the average speed of the flow.[8]

5. ADDITIONAL RESULTS

Field plots of velocity vectors and streamline, vorticity, pressure and temperature contours over the first half of the computed domain, $x = [0, 10]$, are shown in Figure 2, at a time t_T that corresponds to a minimum in the temperature at the position $x = 5{\cdot}0$, $y = 0{\cdot}5$. The absolute value of this time is arbitrary, but for the period shown in Figure 3 it corresponds to $t_T = 0{\cdot}5226$. The rest of the results are all obtained at this value of time. The parabolic velocity profile at $x = 0$ is evident and the velocity at $x = 10$ is never perpendicular to the outflow boundary (shown in detail later. The flow consists of travelling roll cells (waves) whose axes are normal to the x–y plane. At any instant of time, approximately six cells occupy the region of interest; the start-up region of length 1·5–2·0 is evident at the left side of each plot. The length of the start-up region as well as the region of the flow affected by the incorrect outflow conditions can be seen even more clearly in Figure 4. In this figure we plot the maximum velocity components as functions of the longitudinal

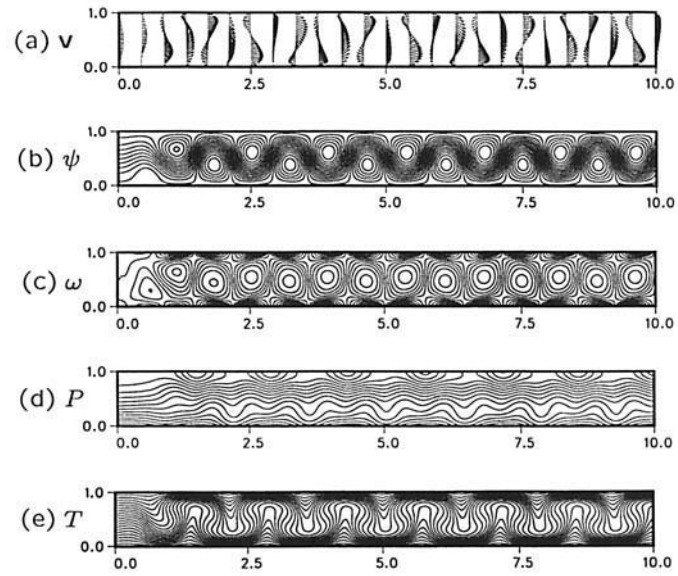

Figure 2. Solution fields at $t=t_T$: (a) v; (b) ψ, $-0{\cdot}6862(0{\cdot}1172)\ 1{\cdot}6578$; (c) ω, $-71{\cdot}45\ (6{\cdot}793)\ 64{\cdot}41$; (d) P, $-65{\cdot}54\ (6{\cdot}106)\ 56{\cdot}58$; (e) T, 0 (0·05) 1

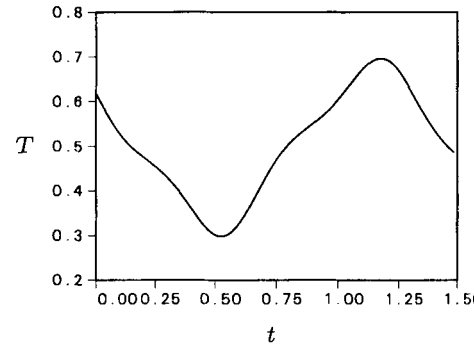

Figure 3. Temperature sample at $(x, y)=(5, 0{\cdot}5)$

co-ordinate. It can be readily seen that the incorrect outflow boundary condition corrupts the flow up to about four vertical heights upstream of the outflow. Note that in the figure the symbols represent the locations of the maxima at t_T, but since the rolls are convected downstream, the maxima occur for all values of x during one period. This last point is noted by passing a line through the symbols in the figure. As can be seen from Table I, the vertical velocity appears to be antisymmetric, since $v_{\max} \approx -v_{\min}$, although the y-positions of the maxima and minima do not occur at $y=0{\cdot}5$. We note (not shown) that the excursions of temperature and vertical velocity component about the mid-height of the channel are antisymmetric. Also noted and shown in Table I is the fact that the retrograde motion within a roll is not as lage as the motion in the $+x$-direction ($|u_{\max}| > |u_{\min}|$). This is due to the fact that forced convection is superimposed on the

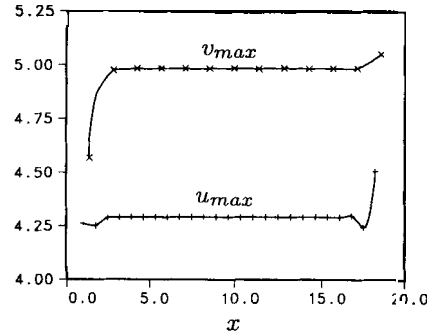

Figure 4. Maxima in u- and v-components of velocity and the longitudinal positions of these maxima at $t = t_T$ as functions of the longitudinal co-ordinate: +, u_{max}; ×, v_{max}

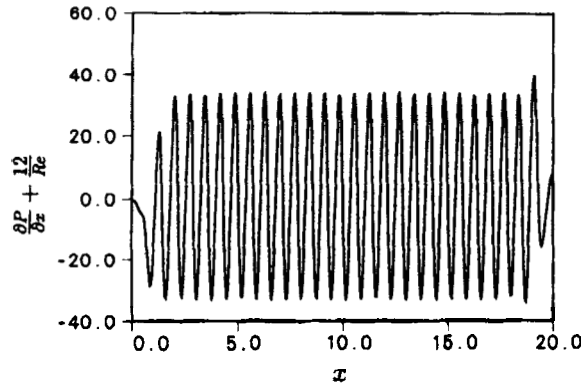

Figure 5. Periodic component of longitudinal pressure gradient at $y = 0{\cdot}5$ and $t = t_T$ as a function of the longitudinal co-ordinate

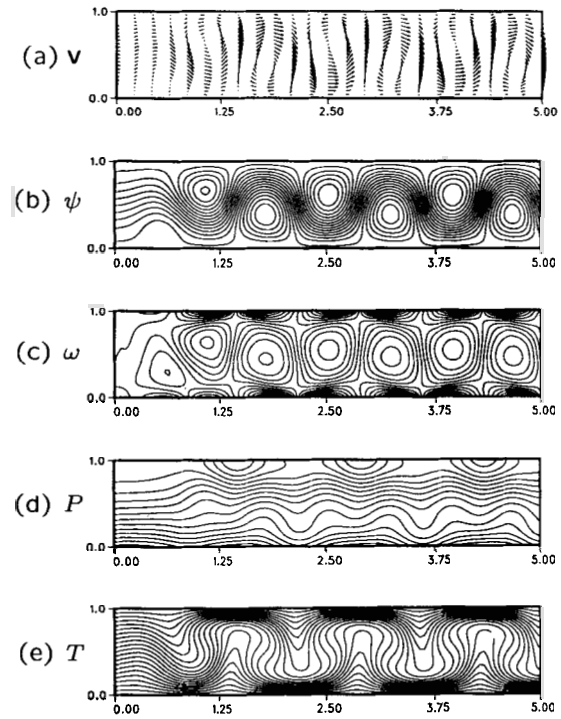

Figure 6. Solution fields at $t = t_T$: (a) v; (b) ψ, $-0{\cdot}6862$ ($0{\cdot}1172$) $1{\cdot}6578$; (c) ω, $-71{\cdot}45$ ($6{\cdot}793$) $64{\cdot}41$; (d) P, $-65{\cdot}54$ ($6{\cdot}106$) $56{\cdot}58$; (e) T, 0 ($0{\cdot}05$) 1

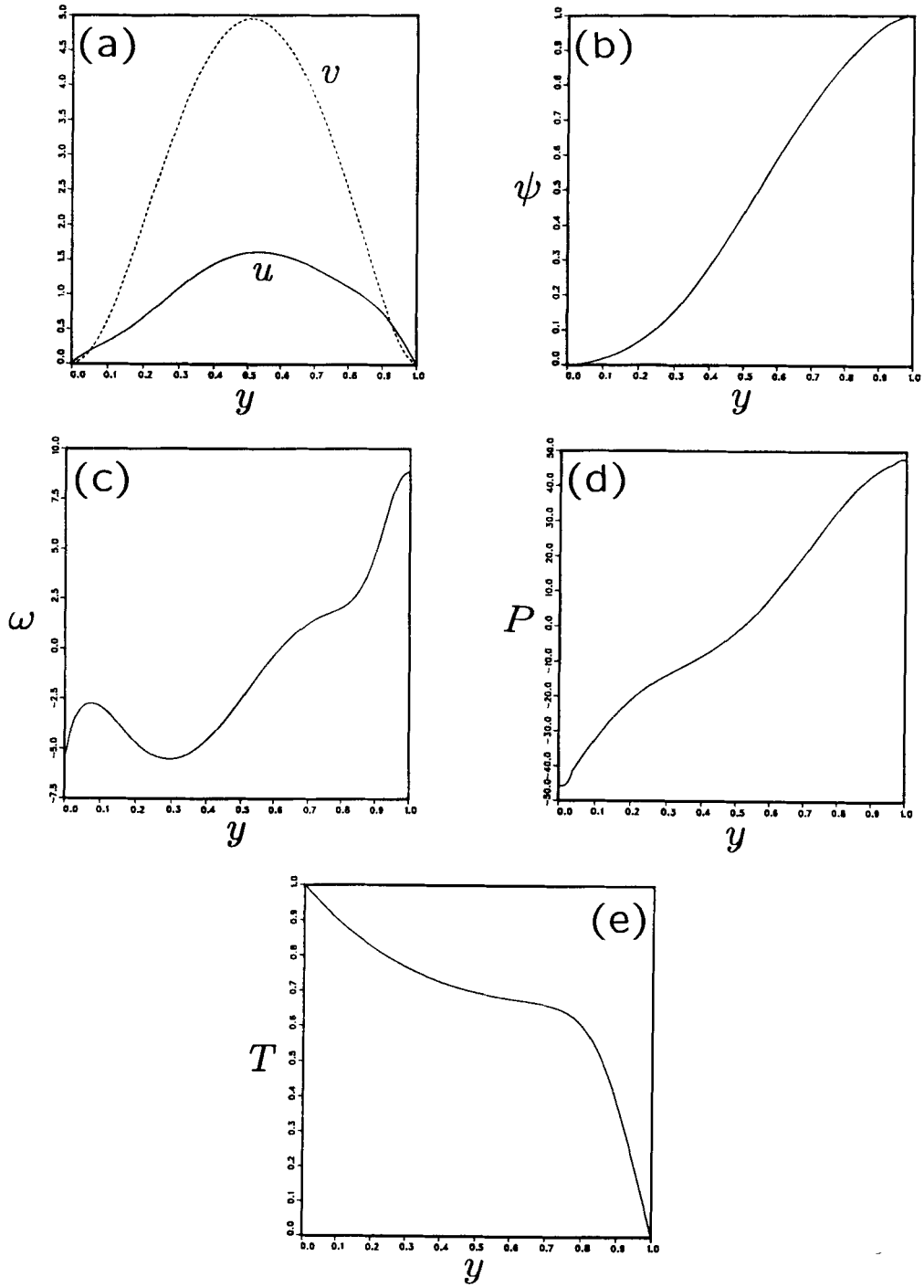

Figure 7. Distributions at $x=10$ and $t=t_T$ as functions of y: (a) ——, u and – – –, v; (b) ψ; (c) ω; (d) P; (e) T

motion owing to the thermal instability. Close examination of the pressure contours in Figure 2(d) reveals that the pressure field is not periodic. However, as shown in Figure 5, a periodic component is superimposed on the overall constant pressure gradient in the x-direction that corresponds to the Poiseuille flow ($dP/dx = -12/Re$). The figure shows the periodic component at $y = 0{\cdot}5$ as a function of longitudinal position in the channel at time t_T. We note (not shown) that the amplitude of the pressure oscillations is a function of the y co-ordinate. In Figure 6, enlargements of the same field plots of Figure 2 are shown over the domain $x = [0, 5]$.

In Figure 7 we present profiles of velocity, streamfunction, vorticity, pressure and temperature across the plane $x = 10$ at time t_T. In addition, in Figure 8 we display the distributions of $\partial u/\partial x$, $\partial v/\partial x$, $\partial P/\partial x$ and $\partial T/\partial x$ at the same location. The corresponding profiles and distributions at the plane $x = 5$ are given in Figures 9 and 10. It is hoped that such results provide sufficient useful information for selecting proper outflow boundary conditions. Note that both the x- and y-components of velocity are positive at $x = 10$ whereas at $x = 5$, u is positive and v is negative across the entire plane. The profiles of vorticity at both planes are quite complex.

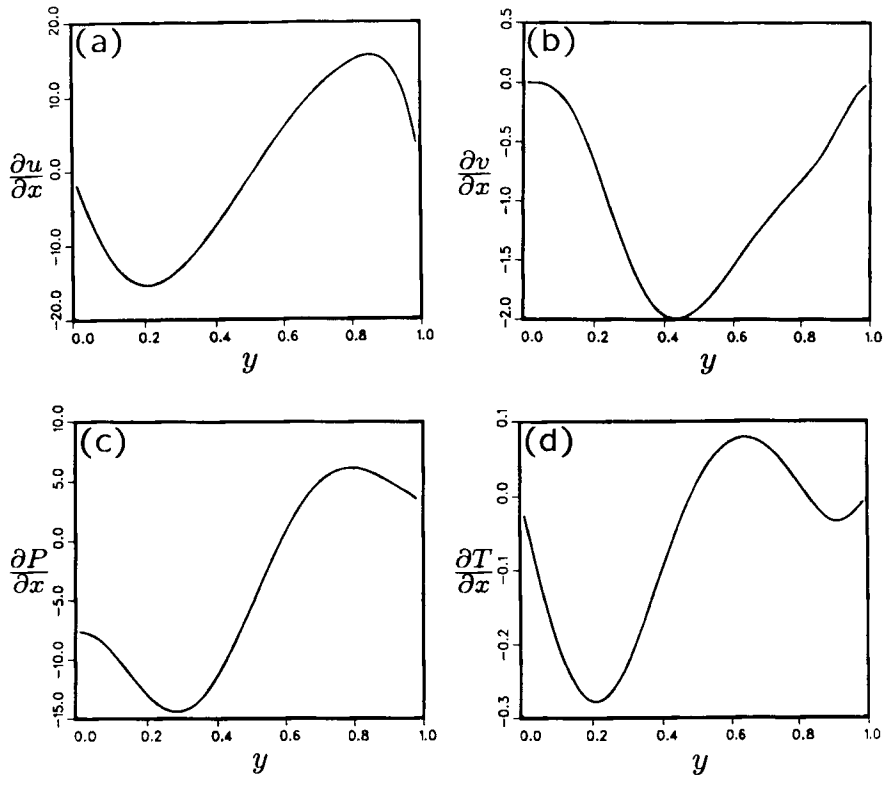

Figure 8. Distributions of longitudinal derivatives at $x = 10$ and $t = t_T$ as functions of y: (a) $\partial u/\partial x$; (b) $\partial v/\partial x$; (c) $\partial P/\partial x$; (d) $\partial T/\partial x$

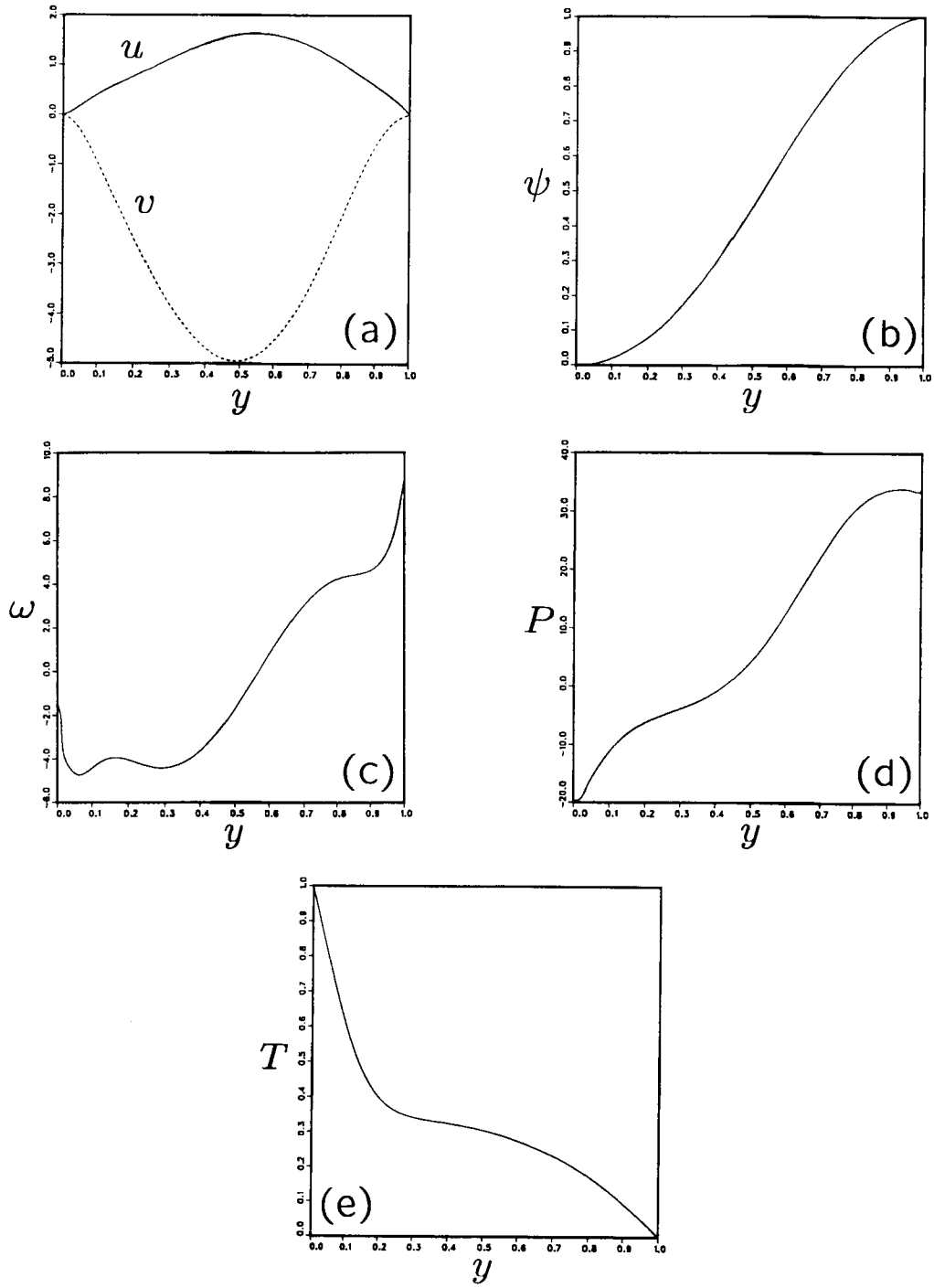

Figure 9. Distributions at $x=5$ and $t=t_T$ as functions of y: (a) ——, u and – – –, v; (b) ψ; (c) ω; (d) P; (e) T

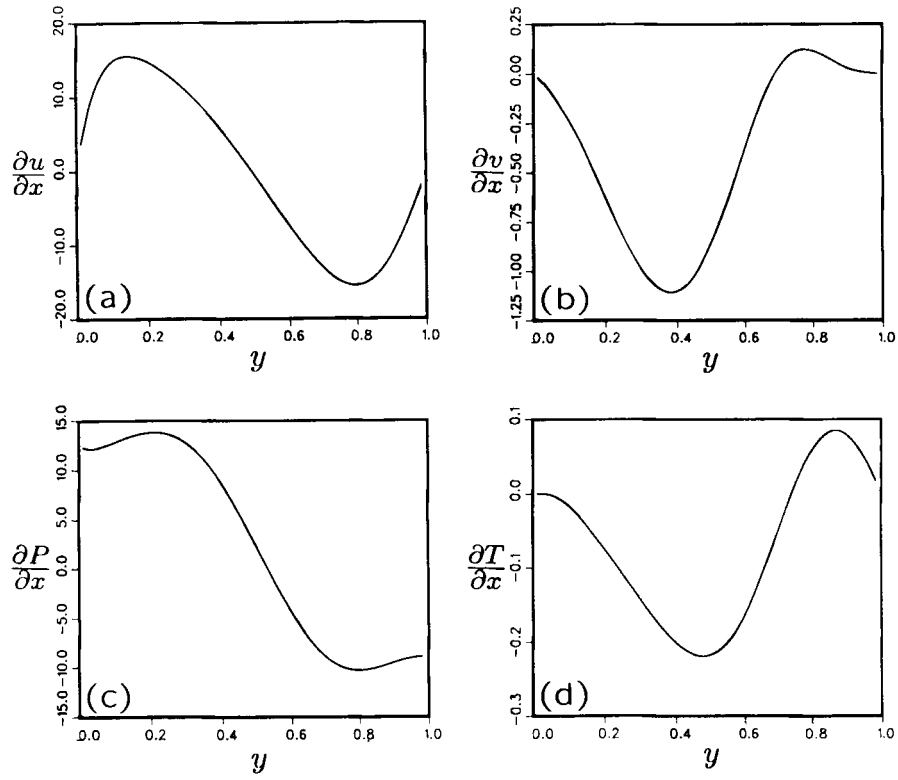

Figure 10. Distributions of longitudinal derivatives at $x=5$ and $t=t_T$ as functions of y: (a) $\partial u/\partial x$; (b) $\partial v/\partial x$; (c) $\partial P/\partial x$; (d) $\partial T/\partial x$

6. CONCLUSIONS

A proposed benchmark solution of a time-dependent fluid flow and heat transfer problem that exhibits strong buoyancy effects coupled to a base-forced flow has been presented for the purpose of testing outflow boundary conditions. Results from five independent numerical computations have been used in a Richardson extrapolation procedure to obtain a solution that is accurate to third order in time and sixth order in space. The results of the extrapolated solution agree with those of the finest grid and time step numerical solution to within 2%. The solution was obtained on an extended domain so that minimal effects of the outflow boundary conditions used in the solution algorithm would occur in the proposed test domain. Tabulated quantities, field plots and profiles of the dependent variables at two axial locations have been presented to provide the information needed for the evaluation of the impact of outflow boundary conditions on the solution within the computational domain.

ACKNOWLEDGEMENT

This work was partially supported by the U.S. Department of Energy under Contract No. DE-AC04-76DP00789.

REFERENCES

1. B. J. Curtis and J. P. Dismukes, 'Effects of natural and forced convection in vapor phase growth systems', *J. Cryst. Growth*, **17**, 128–140 (1972).
2. L. J. Giling, 'Gas flow patterns in horizontal epitaxial reactor cells observed by interference holography', *J. Electrochem. Soc.*, **129**, 634–644 (1982).
3. K. F. Jensen, 'Modeling of chemical vapor deposition reactors', *Proc. 9th Int. Conf. on Chemical Vapor Deposition*, The Electrochemical Society, Pennington, New Jersey, 1984, pp. 3–20.
4. K. C. Chiu and F. Rosenberger, 'Mixed convection between horizontal plates—1. Entrance effects', *Int. J. Heat Mass Transfer*, **30**, 1645–1654 (1987).
5. G. W. Cullen (ed.), *Proc 10th Int. Conf. on Chemical Vapor Deposition*, The Electrochemical Society, Pennington, New Jersey, 1987, pp. 11–32, 175–180, 193–203.
6. H. Moffat and K. F. Jensen, 'Three-dimensional flow effects in silicon CVD in horizontal reactors', *J. Electrochem. Soc.*, **135**, 459–471 (1988).
7. K. S. Gage and W. H. Reid, 'The stability of thermally stratified plane Poiseuille flow', *J. Fluid Mech.*, **33**, 21–32 (1968).
8. J.-M. Luijkx, J. K. Platten and J. C. Legros, 'On the existence of thermoconvective rolls, transverse to a superimposed mean Poiseuille flow', *Int. J. Heat Mass Transfer*, **24**, 1287–1291 (1981).
9. J. K. Platten and J. C. Legros, *Convection in Liquids*, Springer, Berlin, 1984, Chap. 8.
10. M. T. Ouazzani, J. P. Caltagirone, G. Meyer and A. Mojtabi, 'Etude numerique et experimentale de la convection mixte entre deux plans horizontaux a temperatures differentes', *Int. J. Heat Mass Transfer*, **32**, 261–269 (1989).
11. G. Evans and R. Greif, 'A study of traveling wave instabilities in a horizontal channel flow with applications to chemical vapor deposition', *Int. J. Heat Mass Transfer*, **32**, 895–911 (1989).
12. A. D. Gosman and W. M. Pun, 'Calculation of recirculating flow', *Lecture Notes*, Imperial College of Science and Technology, London, 1973.
13. S. V. Patankar, *Numerical Heat Transfer and Fluid Flow*, McGraw-Hill, New York, 1980.
14. G. De Vahl Davis, 'Natural convection of air in a square cavity: a benchmark numerical solution', *Int. j. numer. methods fluids*, **3**, 249–264 (1983).
15. S. W. Churchill, P. Chao and H. Ozoe, 'Extrapolations of finite-difference calculations of laminar natural convection in enclosures to zero grid size', *Numer. Heat Transfer*, **4**, 39–51 (1981).